Earth and Planetary Science Letters 411 (2015) 121–130

Contents lists available at ScienceDirect

Earth and Planetary Science Letters

www.elsevier.com/locate/epsl

On the relationship between volcanic hotspot locations, the reconstructed eruption sites of large igneous provinces and deep mantle seismic structure

D.R. Davies [a,*], S. Goes [b], M. Sambridge [a]

[a] Research School of Earth Sciences, The Australian National University, Canberra, Australia
[b] Department of Earth Science and Engineering, Imperial College, London, UK

ARTICLE INFO

Article history:
Received 4 June 2014
Received in revised form 25 November 2014
Accepted 29 November 2014
Available online xxxx
Editor: Y. Ricard

Keywords:
mantle plumes
hotspot volcanism
large igneous provinces
LLSVPs
thermo-chemical piles

ABSTRACT

It has been proposed that volcanic hotspots and the reconstructed eruption sites of large igneous provinces (LIPs) are preferentially located above the margins of two deep mantle large low shear-wave velocity provinces (LLSVPs), beneath the African continent and the Pacific Ocean. This spatial correlation has been interpreted to imply that LLSVPs represent long-lived, dense, stable thermo-chemical piles, which preferentially trigger mantle plumes at their edges and exert a strong influence on lower-mantle dynamics. Here, we re-analyse this spatial correlation, demonstrating that it is not global: it is strong for the African LLSVP, but weak for the Pacific. Moreover, Monte Carlo based statistical analyses indicate that the observed distribution of African and Pacific hotspots/reconstructed LIPs is consistent with the hypothesis that they are drawn from a sample that is uniformly distributed across the entire areal extent of each LLSVP: the stronger spatial correlation with the margin of the African LLSVP is expected as a simple consequence of its elongated geometry, where more than 75% of the LLSVP interior lies within 10° of its margin. Our results imply that the geographical distribution of hotspots and reconstructed LIPs does not indicate the extent to which chemical heterogeneity influences lower-mantle dynamics.

1. Introduction and motivation

Geochemistry provides clear evidence for a mantle that is heterogeneous in major- and trace-element composition, with mantle-sourced magmas regularly including recycled plate tectonic material and, occasionally, primitive material dating back to the early Earth (e.g. Hofmann and White, 1982; Zindler and Hart, 1986; Hofmann, 1997, 2003; Tackley, 2007; Davies, 2011; Jackson and Carlson, 2011; Campbell and O'Neill, 2012). However, the distribution, scale and dynamical significance of this heterogeneity remain unclear. Recent debate has focussed upon whether or not the primary seismic features of Earth's lowermost mantle, large low shear-wave velocity provinces (LLSVPs) beneath the African continent and the south-central Pacific Ocean, represent long-lived, dense, discontinuous thermo-chemical piles (e.g. Masters et al., 2000; Forte and Mitrovica, 2001; Tackley, 1998, 2002; Ni et al., 2002; Trampert et al., 2004; McNamara and Zhong, 2005; Garnero and McNamara, 2008; Simmons et al., 2009; Schuberth et al., 2009, 2012; Davies et al., 2012, 2015). If this is the case, their scale and volume would imply that chemical heterogeneity plays a key role in governing lower-mantle dynamics (e.g. McNamara and Zhong, 2005; Deschamps and Tackley, 2008, 2009).

LLSVPs are proposed to be thermo-chemical in nature based upon their: (i) strong shear-wave velocity anomalies; (ii) disparate signatures in shear and compressional-wave velocities; (iii) anti-correlated shear and bulk-sound velocities; (iv) sharp sides, expressed in strong shear-wave velocity gradients; and (v) anti-correlated shear-wave velocity and density anomalies (e.g., Ishii and Tromp, 1999; Masters et al., 2000; Karato et al., 2001; Ni et al., 2002; Trampert et al., 2004; Hernlund and Houser, 2008; Garnero and McNamara, 2008). However, several recent studies demonstrate that the majority of these attributes can be equally well explained by thermal and phase related heterogeneity alone (e.g. Schuberth et al., 2009, 2012; Davies et al., 2012, 2015), which is consistent with earlier studies showing that the lower mantle's long-wavelength structure can be reproduced by thermal subduction history (e.g. Richards and Engebretson, 1992; Ricard et al., 1993). Only an anti-correlation between shear-wave velocity and density anomalies would provide unambiguous evidence for dense chemical heterogeneity. Although some studies have found such an anti-correlation (e.g. Ishii and Tromp, 1999; Trampert et al., 2004), our ability to resolve lower-mantle den-

* Corresponding author.
E-mail address: Rhodri.Davies@anu.edu.au (D.R. Davies).

http://dx.doi.org/10.1016/j.epsl.2014.11.052
0012-821X/

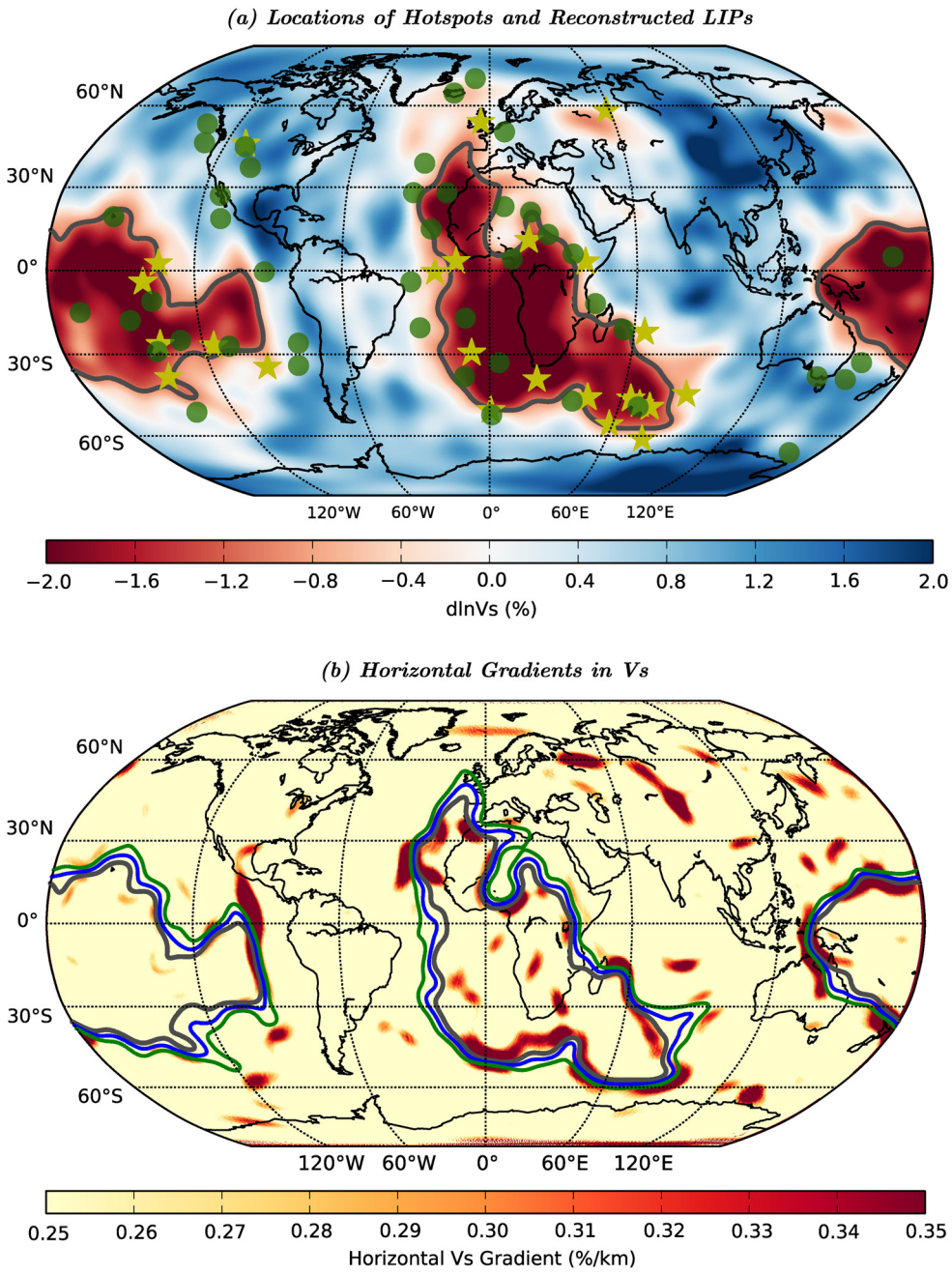

Fig. 1. (a) Surface hotspot locations (Green circles: Steinberger, 2000) and the reconstructed eruption sites of large igneous provinces (Yellow stars: Torsvik et al., 2006, 2008b), plotted above the shear-wave tomography model SMEAN (Becker and Boschi, 2002), at 2800 km depth. The -1.0% $\mathrm{d}\ln V_S$ contour, which approximately outlines large low shear-wave velocity provinces (LLSVPs) beneath Africa and the Pacific, is shown in grey; (b) Magnitude of horizontal shear-wave velocity anomaly gradients from the SMEAN model, at 2800 km depth. The -1.0% $\mathrm{d}\ln V_S$ contour is shown once again (grey), alongside the -0.7% (blue) and -0.4% (green) $\mathrm{d}\ln V_S$ contours. All contours consistently pass through the regions of highest $\mathrm{d}\ln V_S$ gradients at the margins of the African and Pacific LLSVPs. (For interpretation of the references to color in this figure legend, the reader is referred to the web version of this article.)

sity heterogeneity is debated (e.g. Resovsky and Ritzwoller, 1999; Romanowicz, 2001; Masters and Gubbins, 2003). Furthermore, the seismic evidence seems to require that the volume fraction of dense chemical heterogeneity is less than 1–3% of the mantle's volume (Hernlund and Houser, 2008; Davies et al., 2015). Whilst this may be significant in generating geochemical heterogeneity with a range of residence times (e.g. Tackley and Xie, 2002; Huang and Davies, 2007b, 2007a; Brandenburg et al., 2008), it would have a limited influence on the geometry and vigour of lower-mantle dynamics.

An additional and key observation that is often invoked as evidence for the thermo-chemical nature of LLSVPs and, hence, the dynamical significance of chemical piles, is that surface hotspot locations and the reconstructed eruption sites of large igneous provinces (LIPs) appear to concentrate above LLSVP margins (e.g. Thorne et al., 2004; Torsvik et al., 2006, 2008b, 2010; Burke et al., 2008) (Fig. 1a). In a dynamically isochemical mantle, plumes would be expected to rise throughout LLSVP interiors, with no clear preference for their margins (e.g. Davies, 1999). Accordingly, the plume localisation implied by this observation is generally attributed to the interaction of mantle flow with the edges of deep mantle thermo-chemical piles (e.g. Thorne et al., 2004; Torsvik et al., 2006; Tan et al., 2011; Steinberger and Torsvik, 2012; Bower et al., 2013). A recent global Monte Carlo based statisti-

cal study by Austermann et al. (2014), however, has challenged this view, demonstrating that the available sample of reconstructed LIPs is spatially correlated with both LLSVPs and LLSVP margins and that these correlations cannot be statistically distinguished. It is therefore premature to claim that plumes are preferentially generated at LLSVP margins (Austermann et al., 2014).

In this paper, we further analyse the spatial correlation of volcanic hotspot locations and the reconstructed eruption sites of LIPs with LLSVP margins, and specifically test whether results are consistent for the African and Pacific domains. We begin by illustrating the correlation and its sensitivity to a range of parameters, following the approach of Torsvik et al. (2006) (Section 2). However, this conventional approach does not account for statistical effects of small sample sizes, variable sample sizes between the African and Pacific domains and, most significantly, geometrical differences between the elongated African LLSVP and its more rounded Pacific counterpart. Accordingly, in Section 3, we build on the recent study of Austermann et al. (2014), by undertaking Monte Carlo based statistical analyses that overcome these limitations. Our results and their implications for the nature of lower-mantle dynamics are summarised in Section 4.

2. Conventional correlation analyses

For the first part of our analyses, we follow the approach outlined by Torsvik et al. (2006), who assessed the spatial correlation of hotspots and reconstructed LIPs with LLSVP margins by calculating the minimum angular distance between hotspot/reconstructed LIP locations and a specific negative shear-wave velocity anomaly ($\mathrm{d}\ln V_S$) contour, at a chosen depth, in a tomographic model. Our analyses are undertaken globally as well as regionally for hotspots/reconstructed LIPs that are located within the African and Pacific domains (for regional hotspot/reconstructed LIP classification, see Supplementary Fig. 1). We also analyse the sensitivity of results to a range of assumptions, including the choice of tomographic model and the definition of the LLSVP boundary.

2.1. Methods

Individual tomographic models differ in their distribution of deep mantle heterogeneity due to differences in datasets and choices made during the inversion, including parameterisation and regularisation. For this reason, Thorne et al. (2004) utilised six different tomographic models when analysing the correlation between hotspots and deep mantle seismic structure, Torsvik et al. (2006) used the SMEAN model (Becker and Boschi, 2002), which is an amalgamation of three separate pre-2002 models: S20RTS, SB4L18 and NGRAND (Ritsema et al., 1999; Masters et al., 2000; Grand, 2002), whilst Austermann et al. (2014) considered these pre-2002 models separately. We will consider five shear-wave tomography models, derived using distinct datasets and techniques: (i) SMEAN – for direct comparison with the results of Torsvik et al. (2006); (ii) S40RTS (Ritsema et al., 2011) – generated from measurements of Rayleigh-wave phase velocities, teleseismic body-wave travel times and normal-mode splitting functions; (iii) HMSL-06 (Houser et al., 2008) – generated using travel times measured by a cluster analysis of long-period body waveforms; (iv) S362ANI (Kustowski et al., 2008) – an anisotropic model, generated using long-period waveforms and body-wave travel times; and (v) Gypsum-S (Simmons et al., 2010) – generated using body-wave travel times, in conjunction with models for surface plate motions, free-air gravity, dynamic topography and the core–mantle boundary's excess ellipticity.

Dynamically, one would expect plumes to rise from regions with high thermal and/or compositional gradients (e.g. Lowman et al., 2004; Davies, 2005; Zhong, 2006; Davies and Davies, 2009). Hence, Thorne et al. (2004) compared surface hotspot locations with regions of high seismic velocity gradient in the lowermost mantle, inferring a strong correlation. Their analysis also demonstrates that the strongest lateral shear-wave velocity gradients tend to surround LLSVPs. Since LLSVPs are imaged as distinct, coherent structures (e.g. Lekic et al., 2011), isocontours also outline the margin successfully (Torsvik et al., 2006). Motivated by the observation that steep shear-wave velocity gradients in the tomographic model SMEAN lie close to the -1.0% $\mathrm{d}\ln V_S$ contour, this contour was used by Torsvik et al. (2006) to define the LLSVP boundary. However, as demonstrated in Fig. 1(b), other $\mathrm{d}\ln V_S$ contours also pass through the same high seismic velocity gradient regions. Within the limits of tomographic resolution and the lateral variability of this resolution, these contours will yield a comparable approximation to LLSVP boundaries (which is also implied by the different velocity/velocity-gradient LLSVP boundary definitions of Austermann et al., 2014). As such, we analyse the sensitivity of results to the $\mathrm{d}\ln V_S$ contour value (testing values from $\mathrm{d}\ln V_S = -0.1\%$ to -1.0%). Tests were undertaken at 2600, 2700 and 2800 km depth, although results were consistent across all three depths and, hence, they are only presented for the latter.

The sensitivity of results to the angular search tolerance, θ (i.e. the maximum angular distance between a hotspot/LIP and the LLSVP margin that is permitted if the hotspot/LIP is to be classified as a 'margin' hotspot/LIP), is also examined. Torsvik et al. (2006) used $\theta = 10^\circ$, motivated by the numerical models of Steinberger (2000), which predict that plumes can be deflected by up to 10° from their deep mantle source. In our dynamic models, the majority of plumes are deflected by 6–8° at most from their deep mantle source (e.g. Davies and Davies, 2009). Furthermore, the maximum spatial resolution of various global tomography models in the lowermost mantle ranges from ∼5 to 10°. Consequently, θ values ranging from 5 to 10° are examined here.

Finally, hotspot catalogues have their own ambiguities, as different studies impose different selection criteria, leading to catalogues with anything from ∼20 to ∼100 hotspots (e.g. Morgan, 1981; Vogt, 1981; Steinberger, 2000; Courtillot et al., 2003; Montelli et al., 2006; Boschi et al., 2007). However, to allow for direct comparison with the results of Torsvik et al. (2006), we consider the catalogue of Steinberger (2000), which contains 44 hotspots and is constrained by surface observations of age and anomalous buoyancy-flux. Most recent catalogues comprise only slight variations on this catalogue, or include only a subset of the data (such as hotspots underlain by specific seismic expressions: Montelli et al., 2006). The reconstructed eruption sites of LIPs are taken from the catalogue of Torsvik et al. (2006), supplemented by the Skagerrak-Centered LIP (SCLIP) of Torsvik et al. (2008b), with reconstructions based upon the global palaeomagnetic absolute reference frame (note that results should largely be insensitive to the absolute reference frame used: Austermann et al., 2014). This is the most recent and comprehensive reconstructed LIP catalogue available. All hotspot and reconstructed LIP locations are shown in Fig. 1(a). Note that for the remainder of this paper, unless explicitly stated otherwise, when we refer to LIP locations we are referring their reconstructed eruption sites.

2.2. Results

Representative results are shown in Fig. 2, where we display the percentage of 'margin' hotspots and LIPs, as a function of θ, using a range of $\mathrm{d}\ln V_S$ contours from the SMEAN tomographic model at 2800 km depth to define the LLSVP boundary. We present results globally and regionally for the African and Pacific domains. Results for the tomographic models S40RTS (Ritsema et al., 2011), HMSL-06 (Houser et al., 2008), S362ANI (Kustowski et al., 2008)

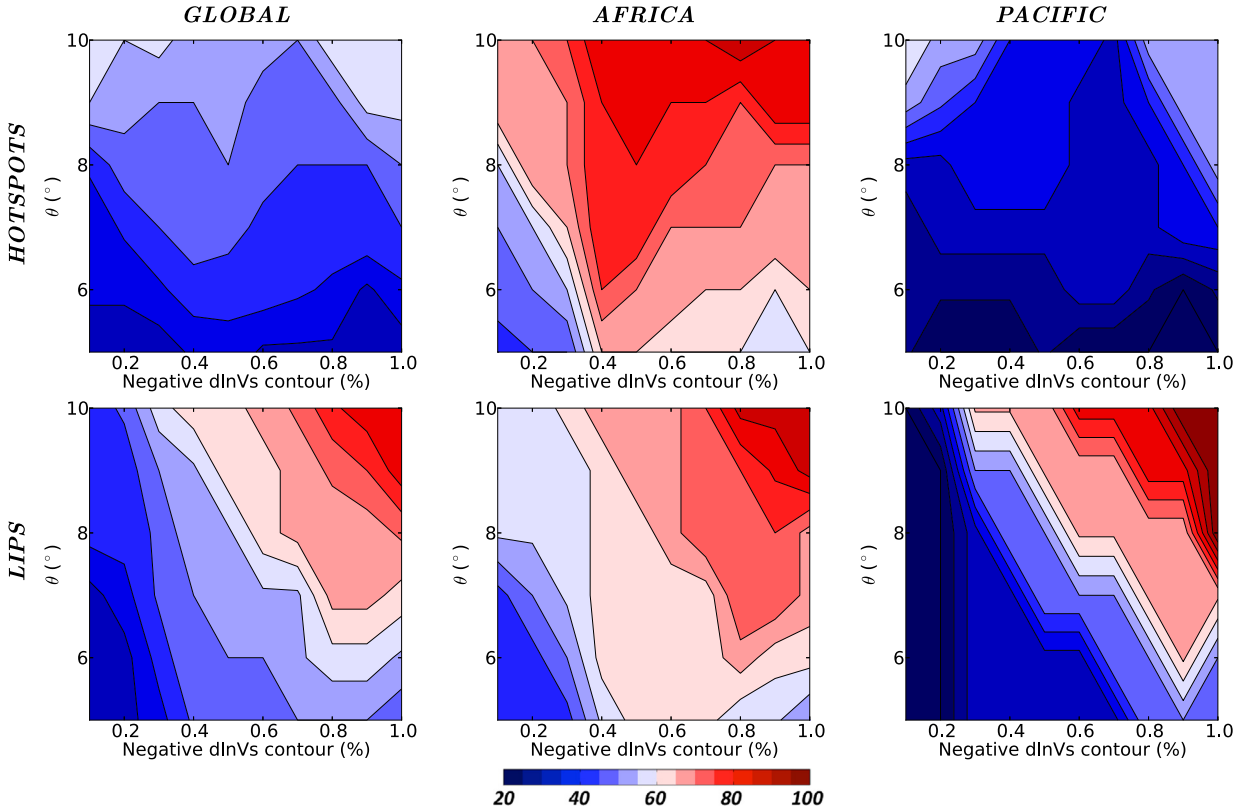

Fig. 2. The percentage of hotspots (top) and LIPs (bottom) located within an angular distance (θ) of LLSVP margins, at 2800 km depth, as delineated by a specific negative $\mathrm{dln}\,V_S$ contour in the SMEAN tomographic model. Note that the results presented here are only a subset of our full analysis – comparative plots for other tomographic models (Houser et al., 2008; Kustowski et al., 2008; Simmons et al., 2010; Ritsema et al., 2011) are presented in Supplementary Figs. 2 and 3. The designation of African and Pacific hotspots and LIPs can be found in Supplementary Fig. 1. The trends shown here, including the significant difference between African and Pacific distributions, are generally consistent across all tomographic models.

and Gypsum-S (Simmons et al., 2010) are presented in Supplementary Figs. 2 and 3.

Torsvik et al. (2006) found that, globally, ~55% of hotspots are located above LLSVP margins, the result shown in Fig. 2 at $\theta = 10°$ and $\mathrm{dln}\,V_S = -1.0\%$. This spatial correlation, however, is reduced to <30% at lower θ and shows substantial regional variability between the African and Pacific domains, with strong correlations generally observed for the former (>80%, at $\theta \geq 8°$) and weak correlations for the latter (<50%, even at high θ). If hotspot locations showed a clear preference for LLSVP margins, one would expect a maximum correlation at the $\mathrm{dln}\,V_S$ value that best represents the margin. However, in the SMEAN results presented in Fig. 2, correlation maxima: (i) occur at different $\mathrm{dln}\,V_S$ contour amplitudes in the African and Pacific domains; and (ii) occur at different $\mathrm{dln}\,V_S$ contour amplitudes for different θ. These trends are not indicative of a clear association with a specific $\mathrm{dln}\,V_S$ contour.

For Africa, all tomographic models predict correlation maxima at different $\mathrm{dln}\,V_S$ amplitudes, which is to be expected, due to the different range of anomalies recovered by each model (Supplementary Fig. 2). Nonetheless, the various tomographic models analysed reveal similar patterns: maximum correlation values of ≥80%, when $\theta \geq 8°$. We therefore conclude that hotspots are more concentrated above the margins of the African LLSVP than within its low-velocity interior. However, for the Pacific domain, hotspot correlations are weak for all tomographic models considered (with values regularly <40–50%, even at the highest θ values) and often without a clear maximum as a function of $\mathrm{dln}\,V_S$ contour amplitude. For the SMEAN model, the strongest correlations are displayed at the lower and upper limits of the $\mathrm{dln}\,V_S$ contour range examined. This is consistent with the map presented in Fig. 1(a), which shows that hotspots occur both above the interior (high $\mathrm{dln}\,V_S$ amplitudes) and above the margins (low $\mathrm{dln}\,V_S$ amplitudes) of the Pacific LLSVP.

The global correlation between reconstructed LIP locations and LLSVP margins is generally stronger than that for hotspots. At $\theta = 10°$ and $\mathrm{dln}\,V_S = -1.0\%$, the result is that of Torsvik et al. (2006), with >80% of LIPs located above LLSVP margins. This global trend, however, is dominated by African LIPs, since 16 of the 24 LIPs examined occur within the African domain (Supplementary Fig. 1). Furthermore, results show a strong dependence on the exact $(\theta, \mathrm{dln}\,V_S)$ combination. If hotspot/LIP locations showed a clear preference for LLSVP margins, and these margins were well-defined, one would expect the maximum in correlation to coincide for both hotspots and LIPs, which is not apparent for the SMEAN model results presented in Fig. 2. Indeed, across all tomographic models considered, there is no consistency between the location of correlation maxima as a function of $\mathrm{dln}\,V_S$ contour amplitude for hotspots and LIPs. Note that results within the Pacific domain should be treated with caution, due to the small LIP sample size (only 6 LIPs occur within the Pacific domain). Again, the major trends described are consistent across all tomographic models examined (Supplementary Fig. 3).

2.3. Summary, limitations, outstanding questions and recent progress

Our re-analysis confirms the result of previous studies (e.g. Burke et al., 2008; Torsvik et al., 2006, 2008b, 2010) that volcanic hotspot locations and the reconstructed eruption sites of LIPs are concentrated above the margins of the African LLSVP. However, this is not the case within the Pacific domain, where hotspot locations show no clear preference for the margins of the underlying LLSVP, whilst the small sample of reconstructed LIPs only shows a pref-

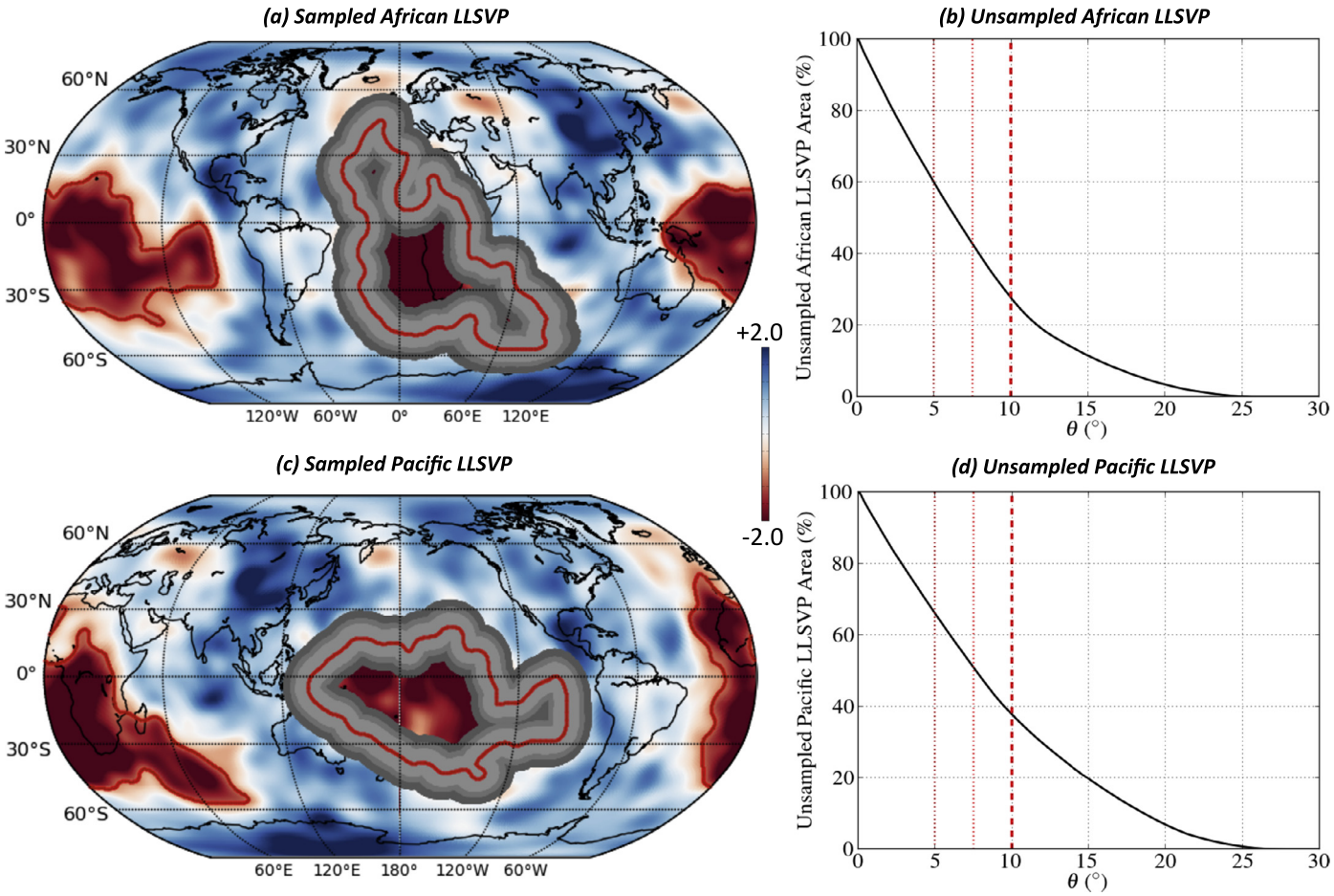

Fig. 3. Regions of the: (a) African; and (c) Pacific LLSVPs that are sampled when using an angular search tolerance of $\theta = 5°$ (light grey), $\theta = 7.5°$ (grey) and $\theta = 10°$ (dark grey), with the -1.0% $\mathrm{dln}\, V_S$ contour of SMEAN (red line) delineating the LLSVP margins, at 2800 km depth. It is noteworthy that if a $\theta = 10°$ criterion is used to quantify the spatial correlation between hotspots/reconstructed LIPs and LLSVP margins (Torsvik et al., 2006), a significant portion of LLSVP interiors is also sampled: 75% of the African, 60% of the Pacific LLSVP (b/d). (For interpretation of the references to color in this figure legend, the reader is referred to the web version of this article.)

erence at specific (θ, $\mathrm{dln}\, V_S$) combinations. Torsvik et al. (2006) place less emphasis on results for the Pacific domain, due to the smaller sample of LIPs and poorer tomographic resolution. This, however, highlights the limitations of this conventional approach of analysing the spatial correlation between hotspot/LIP locations and the margins of deep mantle LLSVPs. Besides not accounting for the statistical effects of small sample sizes and variable sample sizes between the African and Pacific domains, it does not take into account geometrical differences between the elongated African LLSVP and its more rounded Pacific counterpart, which may be a significant factor: as illustrated in Fig. 3, with an angular search tolerance of $\theta = 10°$, a large areal fraction of LLSVP interiors is sampled (i.e. considered 'margin'), with only ∼25% (∼40%) of the African (Pacific) LLSVP interior unsampled (i.e. considered 'interior').

The following questions therefore arise: (i) does the conventional approach reveal a spatial correlation between hotspot/LIPs locations and LLSVP margins or are hotspot/LIP locations actually correlated with LLSVP interiors? (ii) Are such correlations distinguishable? (iii) Could the sampling of a larger areal fraction of the African LLSVP's interior when compared to its Pacific counterpart explain the superior correlations predicted for the African domain? In a recent innovative study, Austermann et al. (2014) showed how a Monte Carlo based sampling approach can be used to address the first two questions. Specifically, 1000 simulations were run, in which 24 points (the global LIP sample size) were randomly positioned on a sphere. LIPs were considered to be spatially correlated with LLSVP margins if their mean angular distance from these margins (8°) was smaller than 95% of the mean angular distances obtained in Monte Carlo sampling. Similarly, LIPs were considered spatially correlated with LLSVPs if the percentage of LIPs overlying LLSVPs (87.5%) was greater than 95% of the percentages obtained via Monte Carlo sampling. Austermann et al. (2014) concluded that: (i) the available sample of reconstructed LIPs is spatially correlated with both LLSVPs and LLSVP margins; and (ii) these correlations cannot be statistically distinguished.

Regional variations in correlation between the African and Pacific domains, however, were not analysed and neither was the spatial correlation between hotspot locations and deep mantle seismic structure. Accordingly, in the following section, we revisit the first two questions separately for the African and Pacific domains and consider both hotspot and LIP data. To additionally answer the third question, we require a sampling strategy that differs to that of Austermann et al. (2014), alongside statistical measures that are more robust than mean angular distances and percentages. We use the Kolmogorov–Smirnov test, which is valid for small and variable sample sizes and provides a robust and quantitative measure of the difference between synthetic and observed distributions.

3. Monte Carlo based statistical analyses

In this section, we present a set of Monte Carlo based statistical analyses of the spatial correlation of hotspots and reconstructed

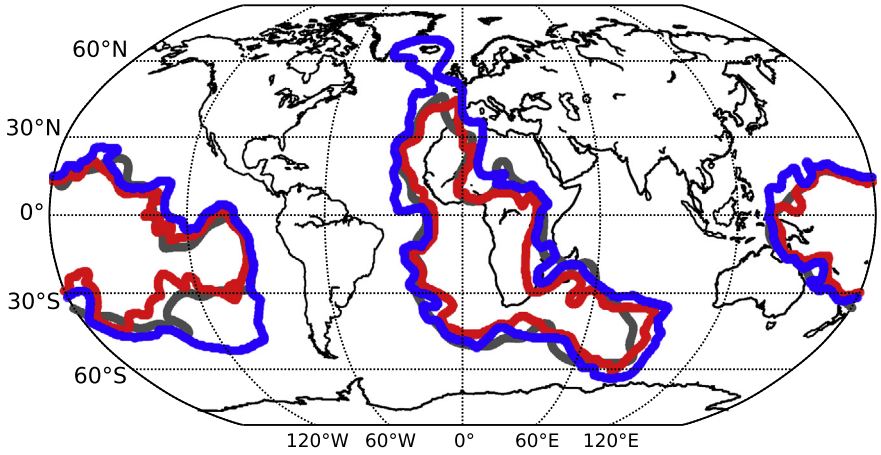

Fig. 4. All tomographic models examined herein (Houser et al., 2008; Kustowski et al., 2008; Simmons et al., 2010; Ritsema et al., 2011), excluding SMEAN (Becker and Boschi, 2002), are combined to yield composite LLSVP boundaries for our Monte Carlo based statistical analyses. Specifically, our boundaries enclose regions where all tomographic models predict $\mathrm{d}\ln V_S$ amplitudes below a threshold value of −0.1% (blue contour), −0.3% (not shown) or −0.5% (red contour), at 2800 km depth. These contours share many characteristics with the $-1.0\%\ \mathrm{d}\ln V_S$ contour of the tomographic model SMEAN, shown in grey. The $\mathrm{d}\ln V_S = -0.1\%$ composite boundary encloses a larger area, extending an additional ∼30° towards the South American continent in the south-eastern Pacific and a further ∼25° towards Iceland at the African LLSVPs northern margin, whilst the $\mathrm{d}\ln V_S = -0.5\%$ boundary mostly falls inside the $-1.0\%\ \mathrm{d}\ln V_S$ contour of SMEAN. (For interpretation of the references to color in this figure legend, the reader is referred to the web version of this article.)

LIPs with: (i) the full areal extent of LLSVPs; and (ii) LLSVP margins. Our analyses are applied separately to the African and Pacific domains.

3.1. Methods

It would be computationally prohibitive to apply these analyses to all tomographic models and $(\theta, \mathrm{d}\ln V_S)$ combinations. Instead, we identify structures and seismic characteristics common to the tomographic models examined herein, to define composite LLSVP boundaries. Specifically, our boundaries enclose regions at 2800 km depth where all tomographic models find $\mathrm{d}\ln V_S$ amplitudes that are less than a threshold value. Our reference case has a $\mathrm{d}\ln V_S$ threshold of −0.1%, although we test the sensitivity of results to this choice by considering different threshold values of −0.3% and −0.5%. Note that our composite model excludes SMEAN, as it is an amalgamation of older models, including S20RTS, which has since been updated to S40RTS. Nonetheless, as illustrated in Fig. 4, our composite boundaries share many characteristics with the $-1.0\%\ \mathrm{d}\ln V_S$ contour of the SMEAN tomographic model. With these LLSVP boundary definitions, we ask the following questions (independently for the African and Pacific domains):

1. Are the observed locations of hotspots and LIPs drawn from a sample where plumes are uniformly distributed across the LLSVP's entire areal extent?
2. Are the observed locations of hotspots and LIPs drawn from a sample where plumes occur within a specified angular distance, θ, of the LLSVP margin?
3. Can our statistical analyses reject either scenario? If not, is one more likely than the other?

To address these questions, we first compute a set of synthetic cumulative distribution functions (CDFs). These CDFs, which represent the areal fraction of the LLSVP that occurs within an angular distance of the LLSVP margin, are subsequently compared to the observed distribution of hotspots and LIPs.

The first case is modelled by uniformly distributing 10^6 points across the entire areal extent of the African (Pacific) LLSVP. To allow for plume tilting (e.g. Steinberger, 2000; Davies and Davies, 2009), an external θ tolerance of 5, 7.5 or 10° is added to our composite boundary. For each point, we calculate the minimum angular distance from the LLSVP margin and, subsequently, construct synthetic CDFs, which are shown for the composite $\mathrm{d}\ln V_S = -0.1\%$ boundary in Fig. 5 (a, c: continuous blue lines). To address the second question, we follow an identical approach, although in this case points are uniformly distributed within a specified angular distance ($\theta = 5, 7.5$ or 10°) of the LLSVP margin (Fig. 5a, c: dashed red lines).

Next, we test whether the observed distributions of hotspots and reconstructed LIPs differ significantly from the synthetic (uniform/margin) distributions, or if they are consistent with the variations that would naturally occur in different samples drawn from these distributions. The difference between two CDFs can be measured in a number of ways. The non-parametric Kolmogorov–Smirnov (K-S) test uses a particularly simple measure: the maximum value of the absolute difference between two CDFs: the K-S statistic (e.g. Kolmogorov, 1933; Corder and Foreman, 2011). What makes the K-S statistic useful is that its distribution in the case of the null hypothesis (i.e. that datasets are drawn from the same distribution) can be calculated to a useful approximation, thus giving the significance of any observed non-zero value. Furthermore, it is valid with small sample sizes, like those considered here.

Results from K-S tests against synthetic uniform and margin distributions, at $\theta = 5, 7.5$ and 10°, for both hotspots and LIPs, are presented in Fig. 5(b, d). The K-S probability values are calculated to answer the following question: if the two distributions were randomly sampled from identical populations, what is the probability that the two cumulative frequency distributions would be as far apart as observed? More precisely, what is the chance that the value of the K-S statistic would be as large as, or larger than, that observed? If the K-S statistic is larger than a critical value (or alternatively, if the K-S probabilities are smaller than a critical value), it can be concluded that the two distributions were sampled from populations with different distributions and, accordingly, the null hypothesis can be ruled out. Our critical values are taken from Zwillinger (2011), at a significance level of 0.05.

3.2. Results

Focussing initially on results for the African domain (Fig. 5b), we see that across all θ values considered: (i) it is not possible to rule out the hypothesis that hotspots and LIPs are drawn from a sample where plumes are uniformly distributed across the en-

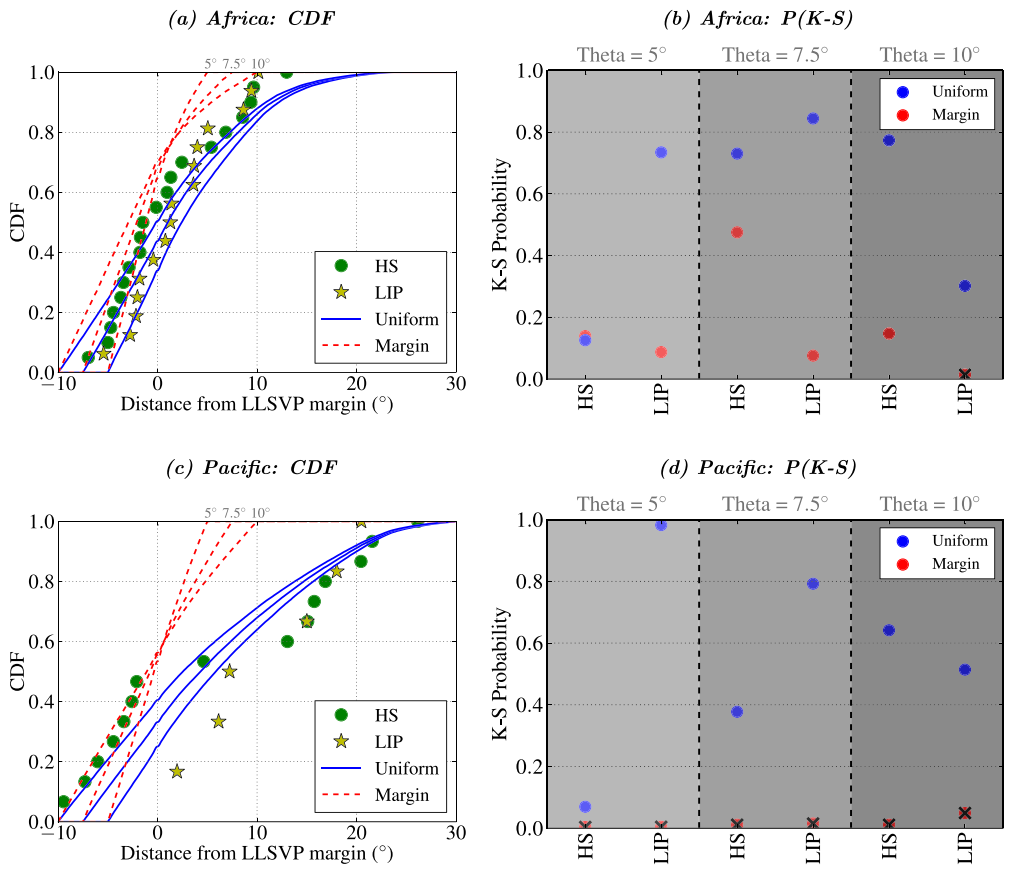

Fig. 5. (a)–(c) Cumulative Distribution Functions (CDF) for hotspots (HS) (Steinberger, 2000) and LIPs (Torsvik et al., 2006, 2008b) as a function of angular distance from the composite $\mathrm{dln}\, V_S = -0.1\%$ contour shown in Fig. 4, alongside synthetic distributions, where plumes are uniformly distributed across the entire areal extent of LLSVPs (continuous blue lines) or uniformly distributed within a specified angular distance ($\theta = 5°$, 7.5° and 10°) of the LLSVP margin (dashed red lines). Angular distances are positive inside and negative outside LLSVPs. (b)–(d) Results from Kolmogorov–Smirnov (K-S) tests, which quantify the probability that the observed hotspot/LIP distributions are drawn from synthetic uniform (blue) or margin (red) distributions. If the K-S probability is less than a critical value, the null hypothesis (i.e. that the observed and synthetic distributions are drawn from identical distributions) can be rejected. Such cases are marked by a black cross, with critical values determined at a significance level of 0.05. (For interpretation of the references to color in this figure legend, the reader is referred to the web version of this article.)

tire areal extent of the LLSVP, as K-S probabilities always exceed critical $P(K\text{-}S)$ values; and (ii) the probability that hotspots and LIPs are drawn from a sample where plumes are uniformly distributed across the entire areal extent of the LLSVP is consistently higher than the probability that hotspots and LIPs are drawn from a sample where plumes occur within a specified angular distance, θ, of the LLSVP margin, excluding $\theta = 5$, where the probability that hotspots are drawn from a uniform sample is similar to a margin sample. Note that the hypothesis that LIPs are drawn from a sample where plumes occur exclusively within 10° of the LLSVP margin can be ruled out: $P(K\text{-}S)$ for this case is less than the critical value applicable at this sample size.

Similar trends are observed for the Pacific domain (Fig. 5d). For all θ values considered, it is not possible to rule out the hypothesis that hotspots and LIPs are drawn from a sample where plumes are uniformly distributed across the entire areal extent of the LLSVP. However, without exception, the hypothesis that hotspots and LIPs are drawn from a sample where plumes occur within a specified angular distance of the LLSVP margin is always ruled out (unsurprisingly therefore, the probability that hotspots and LIPs are drawn from a sample where plumes are uniformly distributed across the entire areal extent of the LLSVP is consistently higher than the probability that hotspots and LIPs are drawn from a sample where plumes occur within a specified angular distance of the LLSVP margin).

Taken together, these results support the view that hotspot and reconstructed LIP locations cannot be distinguished from a distributed set across the entire areal extent of both the African and Pacific LLSVPs. However, results are sensitive to the exact location of the LLSVP boundary. To illustrate the sensitivity of results to this choice, we have computed K-S probabilities for composite contours with threshold values of $\mathrm{dln}\, V_S = -0.3\%$ and $\mathrm{dln}\, V_S = -0.5\%$, with results presented in Fig. 6. Our calculations demonstrate that as the amplitude of the $\mathrm{dln}\, V_S$ threshold value increases: (i) LLSVP areas decrease; (ii) the ratio between the areal extent of the LLSVP margin and its interior increases; and (iii) K-S probabilities are modified, with margin probabilities generally increasing and uniform probabilities generally decreasing. Indeed, at these threshold values, the probability that hotspots/LIPs are drawn from a sample where plumes are uniformly distributed across the entire areal extent of LLSVPs is not always higher than the probability that hotspots/LIPs are drawn from a sample where plumes occur within a specified angular distance of the LLSVP margin.

For the African domain (Fig. 6a, b), $P(K\text{-}S)$ values for the $\mathrm{dln}\, V_S = -0.3\%$ and -0.5% threshold contours are reasonably consistent for synthetic uniform and margin distributions. In only one case is it possible to rule out the hypothesis that hotspots/LIPs are drawn from uniform sample across the entire areal extent of the African LLSVP. However, in this case, the margin hypothesis is also ruled out. In addition, where margin probabilities are high, uniform probabilities are also generally high. This should be no surprise: as the amplitude of the $\mathrm{dln}\, V_S$ threshold value increases, the areal extent of the LLSVP margin and its interior become similar and, hence, distinguishing between both becomes difficult. Within

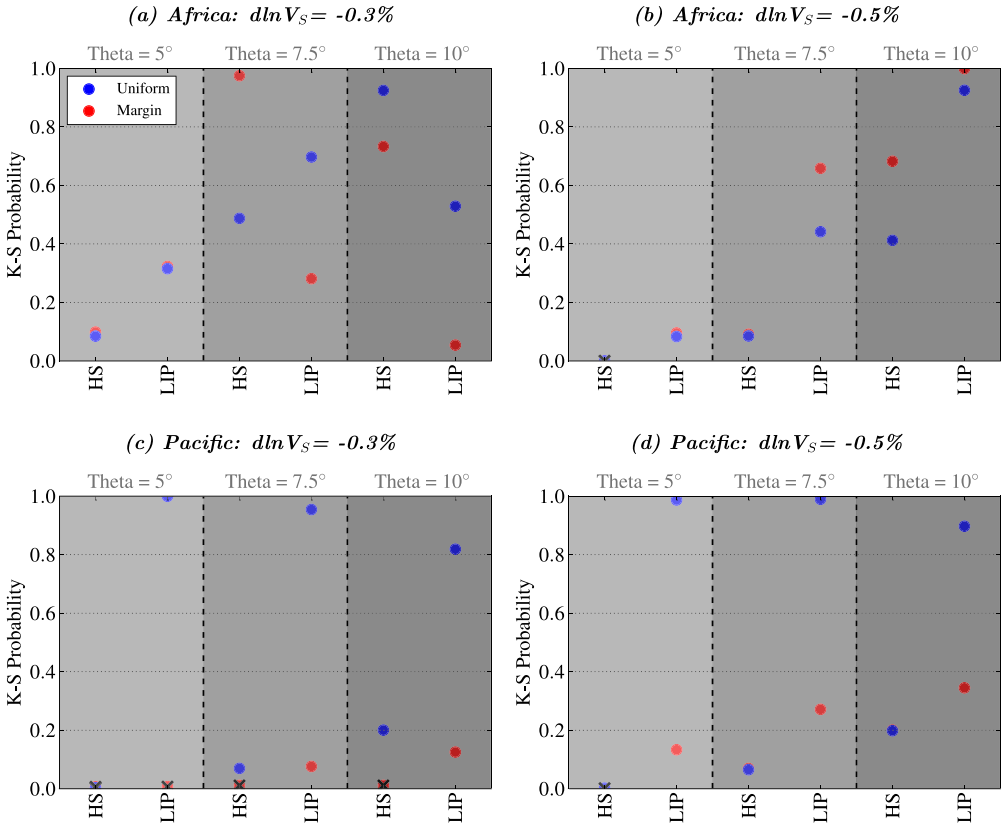

Fig. 6. Results from Kolmogorov–Smirnov (K-S) tests, which quantify the probability that the observed hotspot (HS)/LIP distributions are drawn from synthetic uniform (blue) or margin (red) distributions. The LLSVP margin is defined by composite $\mathrm{d}\ln V_S = -0.3\%$ and $\mathrm{d}\ln V_S = -0.5\%$ contours, with the -0.5% contour illustrated in Fig. 4. (For interpretation of the references to color in this figure legend, the reader is referred to the web version of this article.)

the Pacific domain (Fig. 6c, d), however, $P(K\text{-}S)$ values for LIPs are significantly higher for a sample that is uniformly distributed across the entire areal extent of the LLSVP than a sample where plumes occur within a specified angular distance of the LLSVP margin. For hotspots, $P(K\text{-}S)$ values for synthetic uniform cases are greater than (Fig. 6c) or equal to (Fig. 6d) $P(K\text{-}S)$ values for synthetic margin cases.

3.3. Summary and limitations

In summary, despite results showing sensitivity to the LLSVP boundary location, across all (θ, composite $\mathrm{d}\ln V_S$) combinations considered, the distribution of hotspots and reconstructed LIPs shows no clear preference for the 'margin' scenario first proposed by Torsvik et al. (2006). Our analyses, undertaken separately for the African and Pacific domains, demonstrate that the hypothesis that hotspots/LIPs are uniformly distributed across the entire areal extent of LLSVPs is equally, or more, probable, thus confirming conclusions from the global analyses of Austermann et al. (2014). Furthermore, our statistical tests demonstrate that the apparent concentration of hotspots/LIPs above the margin of the African LLSVP, illustrated in Section 2, is to be expected as a consequence of its elongated geometry, where more than 75% of the LLSVP interior lies within 10° of its margin (compared to only 60% in the Pacific).

It has been argued that the Pacific LLSVP is more poorly imaged than its African counterpart, due to source–receiver geometry and its location beneath the vast Pacific Ocean (see, for example, Bower et al., 2013, for further discussion) and, hence, spatial correlations with the margin of the Pacific LLSVP carry greater uncertainty. This uncertainty is further compounded for the analysis of reconstructed LIPs as: (i) only 6 LIPs occur within the Pacific domain (Torsvik et al., 2006, 2008b); and (ii) plate motion reconstructions within the Pacific domain carry a larger uncertainty than those surrounding the African continent (e.g. Torsvik et al., 2008a). We note that there are additional uncertainties that have not been quantified herein, including: (i) incomplete knowledge of reconstructed LIP locations with respect to the corresponding arrival site of the plume head at the lithosphere's base; and (ii) whether or not all volcanic hotspots analysed have a deep-mantle source (e.g. Montelli et al., 2006; King, 2007; Conrad et al., 2011; Hwang et al., 2011; Davies and Rawlinson, in press). The sensitivity of results to these factors is an avenue for future research.

4. Conclusions

We have re-analysed the spatial correlation between surface hotspot locations and the reconstructed eruption sites of LIPs with LLSVP margins at depth, using two different approaches. A straightforward correlation analysis, which builds on the work of Torsvik et al. (2006) by analysing the sensitivity of results to a wide range of parameters, confirms the conclusions of previous studies that hotspots/reconstructed LIPs are preferentially located above the margins of the African LLSVP (e.g. Torsvik et al., 2006, 2010; Burke et al., 2008). However, this is not the case within the Pacific domain, where hotspots/reconstructed LIPs show no spatial correlation with the underlying LLSVP margin.

Regional Monte Carlo based statistical analyses, which complement those of Austermann et al. (2014) by accounting for effects relating to the small sample size of hotspots and reconstructed LIPs, variable sample sizes between the African and Pacific domains, and the differential geometries of the elongated African LLSVP and its more rounded Pacific counterpart, demonstrate that the regional variability in correlation for the African and

Pacific domains cannot be attributed to different hotspot/LIP sample sizes. Neither does it require distinct physical processes to be operating within both regions: the stronger spatial correlation of hotspots/reconstructed LIPs with the margin of the African LLSVP is expected as a simple consequence of the LLSVP's elongated geometry, where more than 75% of the LLSVP interior lies within 10° of its margin. We conclude, therefore, that by focussing on global amalgamations of hotspot/reconstructed LIP data, which are dominated by African hotspots/reconstructed LIPs, previous studies have overstated the significance of the spatial correlation between hotspot/reconstructed LIP locations and LLSVP margins: the observed correlation does not require a dynamical process that focusses plumes at LLSVP margins.

Our results imply that the distribution of hotspots and LIPs cannot be used as evidence for the thermo-chemical nature and stability of LLSVPs. This supports the conclusions of numerous studies, which demonstrate that the seismic and dynamical characteristics of LLSVPs reflect their dominantly thermal nature and can be explained in the absence of substantial chemical heterogeneity (e.g. Richards and Engebretson, 1992; Ricard et al., 1993; Forte and Mitrovica, 2001; Simmons et al., 2009; Schuberth et al., 2009, 2012; Styles et al., 2011; Davies et al., 2012, 2015). Nonetheless, we emphasise that, when considered alone, the correlation analyses presented here and in Austermann et al. (2014) do not rule out the presence of dense thermo-chemical piles in the deep mantle beneath Africa and the Pacific. In the thermo-chemical models that we have examined previously (Davies et al., 2012) and those presented elsewhere (e.g. Tan et al., 2011; Bower et al., 2013), plumes rise from the pile interior, the pile margin and, less frequently, away from piles. We note that plumes from the edges of chemical piles can be triggered over shorter time-scales by the action of downwellings and, hence, for short evolution times, models may predict higher concentrations of plumes along pile margins (as is the case in the models of Steinberger and Torsvik, 2012). However, if piles exist on the spatial scale implied by LLSVPs, and are able to remain sequestered in the deep mantle for hundreds of millions of years, they will build up substantial excess temperatures compared to ambient mantle (e.g. Christensen and Hofmann, 1994; Davies et al., 2012). Internal upwellings, in addition to those at the margins, would therefore be required if piles are to release their heat (e.g. Jellinek and Manga, 2002). Consequently, for both long-lived thermo-chemical and thermally dominated LLSVPs, plumes are not expected to show a clear preference for LLSVP margins.

Finally, our results do support the notion of relatively long-lived LLSVPs (Burke et al., 2008; Torsvik et al., 2008b, 2010), as they are consistent with a general correlation of hotspots and LIPs with LLSVPs. However, it should be noted that all 6 Pacific LIPs and 13 of 16 African LIPs analysed (excluding Skagerrak – 300 Ma, the Central Atlantic Magmatic Province – 200 Ma, and the Karoo – 182 Ma) were emplaced in the last 150 Myr. Several studies have demonstrated that recent subduction history is capable of maintaining the African and Pacific LLSVPs, in approximately their present-day configuration, for ∼150 Myr, with or without a contribution from chemical buoyancy (e.g. McNamara and Zhong, 2005; Zhang et al., 2010; Davies et al., 2012; Bower et al., 2013). However, given the small number of LIPs preserved with an age that exceeds 150 Ma, particularly within the Pacific domain, limited constraints are provided on LLSVP geometry and their potential fixity prior to this time (as has been hypothesised by Burke et al., 2008; Torsvik et al., 2008b, 2010, 2014).

Acknowledgements

This work was first submitted in December 2012, when DRD was funded by a Fellowship from NERC (NE/H015329/1). DRD is now funded by an ARC Future Fellowship (FT140101262). Authors benefited from discussion with Gareth Collins, Giampiero Iaffaldano, Ian Campbell, Brian Kennett and Huw Davies. We thank Jerry Mitrovica, an anonymous reviewer and Yanick Ricard (Editor) for detailed and constructive comments. Dan Bower is acknowledged for constructive comments on a previous version of this manuscript.

Appendix A. Supplementary material

Supplementary material related to this article can be found online at http://dx.doi.org/10.1016/j.epsl.2014.11.052.

References

Austermann, J., Kaye, B., Mitrovica, J., Huybers, P., 2014. A statistical analysis of the correlation between large igneous provinces and lower mantle seismic structure. Geophys. J. Int. 197, 1–9

Becker, T.W., Boschi, L., 2002. A comparison of tomographic and geodynamic mantle models. Geochem. Geophys. Geosyst. 3, 2001GC000168.

Boschi, L., Becker, T.W., Steinberger, B., 2007. Mantle plumes: dynamic models and seismic images. Geochem. Geophys. Geosyst. 8, Q10006.

Bower, D.J., Gurnis, M., Seton, M., 2013. Lower mantle structure from paleogeographically constrained dynamic Earth models. Geochem. Geophys. Geosyst. 14, 44–63.

Brandenburg, J.P., Hauri, E.H., van Keken, P.E., Ballentine, C.J., 2008. A multiple-system study of the geochemical evolution of the mantle with force-balanced plates and thermochemical effects. Earth Planet. Sci. Lett. 276, 1–13.

Burke, K., Steinberger, B., Torsvik, T.H., Smethurst, M.A., 2008. Plume generation zones at the margins of large low shear velocity provinces on the core–mantle-boundary. Earth Planet. Sci. Lett. 265, 49–60.

Campbell, I.H., O'Neill, H.C., 2012. Evidence against a Chondritic Earth. Nature 483, 553–558.

Christensen, U.R., Hofmann, A.W., 1994. Segregation of subducted oceanic crust in the mantle. J. Geophys. Res. 99, 19867–19884.

Conrad, C.P., Bianco, T.A., Smith, E.I., Wessel, P., 2011. Patterns of intra-plate volcanism controlled by asthenospheric shear. Nat. Geosci. 4, 317–321.

Corder, G.W., Foreman, D.I., 2011. Nonparametric Statistics for Non-statisticians: A Step-by-Step Approach. Wiley.

Courtillot, V., Davaille, A., Besse, J., Stock, J., 2003. Three distinct types of hotspots in the Earth's mantle. Earth Planet. Sci. Lett. 205, 295–308.

Davies, D.R., Davies, J.H., 2009. Thermally-driven mantle plumes reconcile multiple hotspot observations. Earth Planet. Sci. Lett. 278, 50–54.

Davies, D.R., Goes, S., Davies, J.H., Schuberth, B.S.A., Bunge, H., Ritsema, J., 2012. Reconciling dynamic and seismic models of Earth's lower mantle: the dominant role of thermal heterogeneity. Earth Planet. Sci. Lett. 353–354, 253–269.

Davies, D.R., Goes, S., Lau, H.C.P., 2015. Thermally dominated deep mantle LLSVPs: a review. In: Khan, A., Deschamps, F., Kawai, K. (Eds.), The Earth's Heterogeneous Mantle. Springer.

Davies, D.R., Rawlinson, N., in press. On the origin of recent intra-plate volcanism in Australia. Geology. http://dx.doi.org/10.1130/G36093.1.

Davies, G.F., 1999. Dynamic Earth: Plates, Plumes and Mantle Convection. Cambridge University Press.

Davies, G.F., 2011. Dynamical geochemistry of the mantle. Solid Earth 2, 159–189.

Davies, J.H., 2005. Steady plumes produced by downwellings in Earth-like vigor spherical whole mantle convection models. Geochem. Geophys. Geosyst. 6, Q12001.

Deschamps, F., Tackley, P.J., 2008. Exploring the model space of thermo-chemical convection: (I) principles and influence of the rheological parameters. Phys. Earth Planet. Inter. 171, 357–373.

Deschamps, F., Tackley, P.J., 2009. Searching for models of thermo-chemical convection that explain probabilistic tomography: (II) influence of physical and compositional parameters. Phys. Earth Planet. Inter. 176, 1–18.

Forte, A.M., Mitrovica, J.X., 2001. Deep-mantle high-viscosity flow and thermochemical structure inferred from seismic and geodynamic data. Nature 410, 1049–1056.

Garnero, E.J., McNamara, A.K., 2008. Structure and dynamics of Earth's lower mantle. Science 320, 626–628.

Grand, S.P., 2002. Mantle shear-wave tomography and the fate of subducted slabs. Philos. Trans. R. Soc., Math. Phys. Eng. Sci. 360, 2475–2491.

Hernlund, J.W., Houser, C., 2008. On the statistical distribution of seismic velocities in Earth's deep mantle. Earth Planet. Sci. Lett. 265, 423–437.

Hofmann, A.W., 1997. Mantle geochemistry: the message from oceanic volcanism. Nature 385, 219–229.

Hofmann, A.W., 2003. Sampling mantle heterogeneity through oceanic basalts: isotopes and trace elements. In: Treatise on Geochemistry. Elsevier, pp. 61–101.

Hofmann, A.W., White, W.M., 1982. Mantle plumes from ancient oceanic crust. Earth Planet. Sci. Lett. 57, 421–436.

Houser, C., Masters, G., Shearer, P., Laske, G., 2008. Shear and compressional velocity models of the mantle from cluster analysis of long-period waveforms. Geophys. J. Int. 174, 195–212.
Huang, J., Davies, G.F., 2007a. Stirring in three-dimensional mantle convection models and implications for geochemistry: heavy tracers. Geochem. Geophys. Geosyst. 8, Q07004.
Huang, J., Davies, G.F., 2007b. Stirring in three-dimensional mantle convection models and implications for geochemistry: passive tracers. Geochem. Geophys. Geosyst. 8, Q03017.
Hwang, Y.K., Ritsema, J., van Keken, P.E., Goes, S., Styles, E., 2011. Wavefront healing renders deep plumes seismically invisible. Geophys. J. Int. 187, 273–277.
Ishii, M., Tromp, J., 1999. Normal-mode and free-air gravity constraints on lateral variations in velocity and density of Earth's mantle. Science 285, 1231–1236.
Jackson, M.G., Carlson, R., 2011. An ancient recipe for flood basalt genesis. Nature 476, 316–319.
Jellinek, A.M., Manga, M., 2002. The influence of a chemical boundary layer on the fixity, spacing and lifetime of mantle plumes. Nature 418, 760–763.
Karato, S.-I., Riedel, M.R., Yuen, D.A., 2001. Rheological structure and deformation of subducted slabs in the mantle transition zone: implications for mantle circulation and deep earthquakes. Phys. Earth Planet. Inter. 127, 83–108.
King, S.D., 2007. Hotspots and edge-driven convection. Geology 35, 223–226.
Kolmogorov, A., 1933. Sulla determinazione empirica di una legge di distribuzione. G. Ist. Ital. Attuari 4, 83–91.
Kustowski, B., Exstrom, G., Dziewonski, A.M., 2008. Anisotropic shear-wave velocity structure of the Earth's mantle: a global model. J. Geophys. Res. 113, B06306.
Lekic, V., Cottaar, S., Dziewonski, A., Romanowicz, B., 2011. Cluster analysis of global lower mantle tomography: a new class of structure and implications for chemical heterogeneity. Earth Planet. Sci. Lett. 357, 68–77.
Lowman, J.P., King, S.D., Gable, C.W., 2004. Steady plumes in viscously stratified, vigorously convecting, three-dimensional numerical mantle convection models with mobile plates. Geochem. Geophys. Geosyst. 5, Q01L01.
Masters, G., Gubbins, D., 2003. On the resolution of density within the Earth. Phys. Earth Planet. Inter. 140, 159–167.
Masters, G., Laske, G., Bolton, H., Dziewonski, A.M., 2000. The relative behavior of shear velocity, bulk sound speed, and compressional velocity in the mantle: implications for chemical and thermal structure. In: Earth's Deep Interior. In: AGU Monograph, vol. 171, pp. 63–87.
McNamara, A.K., Zhong, S., 2005. Thermo-chemical structures beneath Africa and the Pacific Ocean. Nature 437, 1136–1139.
Montelli, R., Nolet, G., Dahlen, F.A., Masters, G., 2006. A catalogue of deep mantle plumes: new results from finite-frequency tomography. Geochem. Geophys. Geosyst. 7, Q11007.
Morgan, W.J., 1981. Hotspot tracks and the opening of the Atlantic and Indian oceans. In: The Sea (vol. 7): The Oceanic Lithosphere. John Wiley & Sons, New York, pp. 443–487.
Ni, S.D., Tan, E., Gurnis, M., Helmberger, D.V., 2002. Sharp sides to the African superplume. Science 296, 1850–1852.
Resovsky, J.S., Ritzwoller, M.H., 1999. Regularization uncertainty in density models estimated from normal mode data. Geophys. Res. Lett. 26, 2319–2322.
Ricard, Y., Richards, M.A., Lithgow-Bertelloni, C., LeStunff, Y., 1993. A geodynamic model of mantle mass heterogeneities. J. Geophys. Res. 98, 21895–21909.
Richards, M.A., Engebretson, D.C., 1992. Large-scale mantle convection and the history of subduction. Nature 355, 437–440.
Ritsema, J., van Heijst, H.J., Woodhouse, J.H., 1999. Complex shear velocity structure imaged beneath Africa and Iceland. Science 286, 1925–1928.
Ritsema, J., van Heijst, H.J., Deuss, A., Woodhouse, J.H., 2011. S40RTS: a degree-40 shear velocity model for the mantle from new Rayleigh wave dispersion, teleseismic traveltimes, and normal-mode splitting function measurements. Geophys. J. Int. 184, 1223–1236.
Romanowicz, B., 2001. Can we resolve 3-D density heterogeneity in the lower mantle? Geophys. Res. Lett. 28, 1107–1110.
Schuberth, B.S.A., Bunge, H.-P., Ritsema, J., 2009. Tomographic filtering of high-resolution mantle circulation models: can seismic heterogeneity be explained by temperature alone? Geochem. Geophys. Geosyst. 10, Q05W03.
Schuberth, B.S.A., Zaroli, C., Nolet, G., 2012. Synthetic seismograms for a synthetic Earth: long-period P- and S-wave traveltime variations can be explained by temperature alone. Geophys. J. Int. 200, 1393–1412.
Simmons, N.A., Forte, A.M., Grand, S.P., 2009. Joint seismic, geodynamic and mineral physical constraints on three-dimensional mantle heterogeneity: implications for the relative importance of thermal versus compositional heterogeneity. Geophys. J. Int. 177, 1284–1304.
Simmons, N.A., Forte, A.M., Boschi, L., Grand, S.P., 2010. GyPSuM: a joint tomographic model of mantle density and seismic wave speeds. J. Geophys. Res. 115.
Steinberger, B., 2000. Plumes in a convecting mantle: models and observations for individual hotspots. J. Geophys. Res. 105, 11127–11152.
Steinberger, B., Torsvik, T.H., 2012. A geodynamic model of plumes from the margins of large low shear velocity provinces. Geochem. Geophys. Geosyst. 13, Q01W09.
Styles, E., Davies, D.R., Goes, S., 2011. Mapping spherical seismic into physical structure: biases from 3-D phase-transition and thermal boundary-layer heterogeneity. Geophys. J. Int. 184, 1371–1378.
Tackley, P.J., 1998. Three-dimensional simulation of mantle convection with a thermo-chemical boundary layer: D″? In: Gurnis, M., Wysession, M.E., Knittle, E., Buffet, B.A. (Eds.), The Core–Mantle-Boundary Region. AGU, Washington DC, pp. 231–253.
Tackley, P.J., 2002. Strong heterogeneity caused by deep mantle layering. Geochem. Geophys. Geosyst. 3, 1024.
Tackley, P.J., 2007. Mantle geochemical geodynamics. In: Treatise on Geophysics, vol. 7: Mantle Dynamics. Elsevier, pp. 437–505.
Tackley, P.J., Xie, S., 2002. The thermo-chemical structure and evolution of Earth's mantle: constraints and numerical models. Philos. Trans. R. Soc. Lond. A 360, 2593–2609.
Tan, E., Leng, W., Zhong, S., Gurins, M., 2011. On the location of plumes and mobility of thermo-chemical structures with high bulk modulus in the 3-D compressible mantle. Geochem. Geophys. Geosyst. 12, Q07005.
Thorne, M.S., Garnero, E.J., Grand, S.P., 2004. Geographic correlation between hotspots and deep mantle lateral shear-wave velocity gradients. Phys. Earth Planet. Inter. 146, 47–63.
Torsvik, T.H., Smethurst, M.A., Burke, K., Steinberger, B., 2006. Large igneous provinces generated from the margins of the large low-velocity provinces in the deep mantle. Geophys. J. Int. 167, 1447–1460.
Torsvik, T.H., Muller, R.D., van der Voo, R., Steinberger, B., Gaina, C., 2008a. Global plate motion frames: towards a unified model. Rev. Geophys. 46, 1–44.
Torsvik, T.H., Smethurst, M.A., Burke, K., Steinberger, B., 2008b. Long term stability in deep mantle structure: evidence from the ~300 Ma Skagerrak-Centered Large Igneous Province (the SCLIP). Earth Planet. Sci. Lett. 267, 444–452.
Torsvik, T.H., Burke, K., Steinberger, B., Webb, S.J., Ashwal, L.D., 2010. Diamonds sampled by plumes from the core–mantle-boundary. Nature 466, 352–358.
Torsvik, T.H., van der Voo, R., Doubrovine, P.V., Burke, K., Steinberger, B., Ashwal, L.D., Trünnes, R.G., Webb, S.J., Bull, A.L., 2014. Deep mantle structure as a reference frame for movements in and on the Earth. Proc. Natl. Acad. Sci. 111, 8735–8740.
Trampert, J., Deschamps, F., Resovsky, J., Yuen, D., 2004. Probabilistic tomography maps chemical heterogeneities throughout the lower mantle. Science 306, 853–856.
Vogt, P.R., 1981. On the applicability of thermal conduction models to mid-plate volcanism: comments on a paper by Gass et al. J. Geophys. Res. 86, 950–960.
Zhang, N., Zhong, S.J., Leng, W., Li, Z.X., 2010. A model for the evolution of Earth's mantle structure since the early Paleozoic. J. Geophys. Res. 115, B06401.
Zhong, S., 2006. Constraints on thermochemical convection of the mantle from plume heat flux, plume excess temperature and upper mantle temperature. J. Geophys. Res. 111, B04409.
Zindler, A., Hart, S., 1986. Chemical geodynamics. Annu. Rev. Earth Planet. Sci. 14, 493–571.
Zwillinger, D., 2011. Standard Mathematical Tables and Formulae, 32nd edition. CRC Press.